

---

# Blocking Ion Migration Stabilizes the High Thermoelectric Performance in Cu<sub>2</sub>Se Composites

Dongwang Yang<sup>a,†</sup>, Xianli Su<sup>a,e,†</sup>, Jun Li<sup>a</sup>, Hui Bai<sup>a,b</sup>, Shanyu Wang<sup>c</sup>, Zhi Li<sup>a,e</sup>, Hao Tang<sup>a</sup>,  
Kechen Tang<sup>a</sup>, Tingting Luo<sup>a,b</sup>, Yonggao Yan<sup>a</sup>, Jinsong Wu<sup>a,b</sup>, Jihui Yang<sup>c</sup>, Qingjie Zhang<sup>a</sup>,  
Ctirad Uher<sup>d</sup>, Mercuri. G. Kanatzidis<sup>e</sup> and Xinfeng Tang<sup>a\*</sup>

<sup>a</sup>*State Key Laboratory of Advanced Technology for Materials Synthesis and Processing,  
Wuhan University of Technology, Wuhan 430070, China.*

<sup>b</sup>*Nanostructure Research Centre, Wuhan University of Technology, Wuhan 430070, China.*

<sup>c</sup>*Materials Science and Engineering Department, University of Washington, Seattle,  
Washington 98195, USA.*

<sup>d</sup>*Department of Physics, University of Michigan, Ann Arbor, Michigan 48109, USA.*

<sup>e</sup>*Department of Chemistry, Northwestern University, Evanston, Illinois 60208, USA.*

This is the author manuscript accepted for publication and has undergone full peer review but has not been through the copyediting, typesetting, pagination and proofreading process, which may lead to differences between this version and the [Version of Record](#). Please cite this article as [doi: 10.1002/adma.12003730](https://doi.org/10.1002/adma.12003730).

This article is protected by copyright. All rights reserved.

---

†These authors contributed equally to this work.

Correspondence and requests for materials should be addressed to Jihui Yang

(jihuiy@uw.edu), Mercuri G. Kanatzidis (m-kanatzidis@northwestern.edu), Xinfeng Tang

(tangxf@whut.edu.cn)

## ABSTRACT

The coexistence of fast ionic conduction and high thermoelectric performance in certain mixed ionic-electronic conductors afford new opportunities and challenges beyond the traditional semiconductors and semimetals. However, their applications are limited due to phase instability under a high current density and large temperature difference. Here, we show that the high thermoelectric performance of superionic conductor  $\text{Cu}_2\text{Se}$  is stabilized through regulating the behaviors of  $\text{Cu}^+$  ions and electrons in a Schottky heterojunction between the  $\text{Cu}_2\text{Se}$  host matrix and *in situ* formed  $\text{BiCuSeO}$  nanoparticles. The accumulation of  $\text{Cu}^+$  ions via an ionic capacitive effect at the Schottky junction under the direct current modifies space charge distribution in the electric double layer, exerting an electrostatic field, which blocks the long-range migration of  $\text{Cu}^+$  and produces a drastic reduction of  $\text{Cu}^+$  ion

This article is protected by copyright. All rights reserved.

---

migration in the composite by nearly two orders of magnitude. Moreover, this heterojunction impedes electrons transferring from BiCuSeO to Cu<sub>2</sub>Se, obstructing the reduction reaction of Cu<sup>+</sup> into Cu metal at the interface and hence stabilizes the  $\beta$ -Cu<sub>2</sub>Se phase under a high DC current density and/or a large temperature gradient. Furthermore, incorporation of BiCuSeO in Cu<sub>2</sub>Se optimizes the carrier concentration and intensifies phonon scattering, contributing to the peak figure of merit  $ZT$  value of  $\sim 2.7$  at 973 K and high average  $ZT$  value of  $\sim 1.5$  between 400 K and 973 K for the Cu<sub>2</sub>Se/BiCuSeO composites. This discovery thus provides a new avenue for stabilizing mixed ionic-electronic conduction thermoelectrics, and fresh insights into controlling ion migration in these ionic transport dominated materials including perovskite photovoltaic materials, solid electrolytes, and solid state batteries.

**One sentence summary:** The space charge region in the Schottky junction between the Cu<sub>2</sub>Se host matrix and *in situ* formed BiCuSeO under a direct current causes drastic suppression of Cu<sup>+</sup> ion migration in the composites, and obstructs the reduction reaction of Cu<sup>+</sup> into Cu metal, which, together with the effective regulation of carrier concentration as well as enhanced interfacial phonon scattering, greatly stabilizes the improved thermoelectric performance.

---

## 1. INTRODUCTION

Thermoelectric (TE) materials allow direct solid-state conversion between heat and electricity via the Seebeck and Peltier effects<sup>[1, 2]</sup>. Compared to other energy conversion technologies, thermoelectricity has unique technical merits, such as high reliability, long life, and absence of noise or greenhouse emissions, and finds applications in harvesting industrial waste heat, solar energy, ocean or geothermal energy, heat from automobile exhausts, in powering the deep space probes, as well as managing spot-size distributed cooling of electronic devices and household appliances<sup>[3]</sup>. To date, TE conversion is mainly driven by the development of higher performing, practically stable, and environmentally friendly TE materials. The major scientific and technological challenge is to compete successfully with the established energy conversion technologies and broaden the range of industrial applications of thermoelectricity. The efficiency of a TE material is gauged by its dimensionless figure of merit  $ZT$ , defined as  $ZT = \alpha^2 \sigma T / (\kappa_L + \kappa_e)$ , where  $\alpha$ ,  $\sigma$ ,  $\kappa_L$ ,  $\kappa_e$ , and  $T$  are the Seebeck coefficient, electrical conductivity, lattice thermal conductivity, electronic thermal conductivity, and the absolute temperature, respectively<sup>[1]</sup>.

Among various classes of TE materials, mixed ionic-electronic conductors, such as  $\text{Cu}_2\text{Te}/\text{Cu}_2\text{Se}/\text{Cu}_2\text{S}$ <sup>[4-10]</sup>,  $\text{Zn}_4\text{Sb}_3$ <sup>[11, 12]</sup>,  $\text{Ag}_2\text{Te}/\text{Ag}_2\text{Se}/\text{Ag}_2\text{S}$ <sup>[13-17]</sup>,  $\text{AgCrSe}_2/\text{CuCrSe}_2$ <sup>[18, 19]</sup>,  $\text{Ag}_8\text{MX}_6$  ( $\text{M}=\text{Sn, Ge, Si}$ ;  $\text{X}=\text{Te, Se, S}$ )<sup>[20-22]</sup>, and  $\text{Ag}_9\text{AlSe}_6/\text{Ag}_9\text{GaSe}_6$ <sup>[23-25]</sup>, constitute a unique

---

family<sup>[26]</sup>. In the mixed conductors, ionic migration coexists with high TE performance in the same temperature regime, indicating an inherent link between the two. In the context of the phonon-glass electron-crystal (PGEC) and hybrid-crystal paradigms of the TE materials research, the mobile ions induce static and dynamic disorders causing strong disruptions of phonon spectra and phonon propagation, and give rise to a “phonon-liquid” behavior<sup>[4]</sup>. Meanwhile, the non-mobile rigid sub-lattice constitutes the conduction path for electrons or holes, resulting in an electron-crystal behavior. Attaining high TE performance in mixed ionic-electronic conductors entails a delicate balance among mobile ions, conduction electrons, and lattice phonons. Yet, while the mobile ions play a constructive role in suppressing the lattice thermal conductivity, they also reveal their destructive influence by undermining the stability of the structure under large electric fields or temperature gradients. Given that a large current density and temperature gradient are indispensable for efficient TE power generation and refrigeration, achieving high TE performance while maintaining high structural integrity remains a formidable challenge for applications of mixed conduction thermoelectrics.

Because of their environmental friendliness, low cost of raw materials and high TE performance,  $\text{Cu}_2\text{Se}$  and its derivatives are among the most notable mixed conductor systems. The early studies of  $\text{Cu}_2\text{Se}$ -based compounds date back to the 1960s, when the 3M

---

Corporation developed and patented  $\text{Cu}_{1.97}\text{Ag}_{0.03}\text{Se}$  as a potentially promising TE material<sup>[27]</sup>, the variants of which were tested by other research institutions, including General Atomics Corporation<sup>[28]</sup>, Teledyne<sup>[29]</sup> and the NASA's Jet Propulsion Laboratory<sup>[30, 31]</sup>. In recent years, more in-depth and systematic studies have been reported on  $\text{Cu}_2\text{Se}$  with the aim of optimizing its TE performance<sup>[5, 6]</sup>, improving its chemical stability<sup>[32]</sup>, and developing new synthesis recipes<sup>[7]</sup>. Still, the high mobility of  $\text{Cu}^+$  ions pose a serious risk to the stability of the material under service conditions that involve high voltage and large thermal gradients. The resulting Cu metal precipitates in the samples and the concomitant structural changes lead to a rapid deterioration of the TE performance, which is the reason why research into the TE prospect of  $\text{Cu}_2\text{Se}$  was once abruptly abandoned<sup>[33, 34]</sup>. Currently, researchers are keen to find ways to inhibit the long-range migration of  $\text{Cu}^+$  and thus improve the material's stability. According to the recent work by Qiu *et al.*<sup>[35, 36]</sup>, it is the material-specific chemical potential difference that governs the precipitation of Cu. Consequently, keeping the operational condition of  $\text{Cu}_2\text{Se}$  below a certain voltage threshold seems to be a safe yet passive and ultimately unsatisfactory solution.

Should the long-range migration of  $\text{Cu}^+$  ions be actively inhibited and the carrier concentration self-regulated,  $\text{Cu}_2\text{Se}$ -based materials would have not only excellent TE performance but also good phase stability. This would be extremely conducive to the

---

commercial applications of  $\text{Cu}_2\text{Se}$ . In this study, by *in situ* forming BiCuSeO nanoparticles in  $\text{Cu}_2\text{Se}$ , the  $\text{Cu}^+$  ion modulated electric double layer in the space charge region due to an ionic capacitive effect in the Schottky junction of  $\text{Cu}_2\text{Se}/\text{BiCuSeO}$  interface under the direct current effectively blocks the long-range migration of  $\text{Cu}^+$  ions throughout the entire sample and hinders the precipitation of Cu metal. This consequently stabilizes the high TE performance of polycrystalline  $\text{Cu}_2\text{Se}$  composites under high electric field and large temperature gradient. In addition, the inter-diffusion of Cu vacancies between the  $\text{Cu}_2\text{Se}_{1+x}$  host matrix and BiCuSeO nano phase during the synthesis process efficiently regulates carrier (hole) concentration around the optimal range for a wide series of compositions. Coupled with the enhanced phonon scattering created by the BiCuSeO nano phase, the overall approach solves the dilemma of phase stability and high TE performance.

## 2. RESULTS AND DISCUSSION

Stoichiometric amounts of Cu, Se, and  $\text{Bi}_2\text{SeO}_2$  were mixed and reacted into  $\text{Cu}_2\text{Se}_{1+x} / y\text{BiCuSeO}$  ( $x = 0, 0.005, 0.010, 0.015, 0.020$ ;  $y = 0, 0.05, 0.1, 0.3, 0.5$  mol%) composites by self-propagating high-temperature synthesis (SHS) reactions<sup>[7, 37-39]</sup>, and densified by the plasma activated sintering (PAS). There are two basic control parameters in this work: the Se excess amount “x” (a.k.a. Cu vacancy) and the mole fraction “y” of BiCuSeO. The relative density of the composite sample is about 95% of the theoretical value, 1~2% lower than that

---

of the pristine material. The primary phase of all samples at room temperature was confirmed to be  $\alpha$ - $\text{Cu}_2\text{Se}$ <sup>[40]</sup>. The presence of the BiCuSeO phase was verified by X-ray diffraction (XRD) measurements in samples with a significant content of BiCuSeO (e.g.,  $y = 0.5$  mol%) (Figure S1), which documented the crucial role of  $\text{Bi}_2\text{SeO}_2$  in the SHS reaction with Cu and Se to form the BiCuSeO compound<sup>[39]</sup>.

The as-formed  $\text{Cu}_2\text{Se}_{1+x} / y\text{BiCuSeO}$  composites exhibit excellent TE properties (Figures S2 – S19). Incorporation of BiCuSeO in the  $\text{Cu}_2\text{Se}$  matrix improves the TE properties dramatically. The peak  $ZT$  values ( $ZT_{\text{peak}}$ ) of a wide range of composites are above 2 at 973 K (Figure S2). Specifically, the  $ZT_{\text{peak}}$  values of  $\text{Cu}_2\text{Se}_{1.005} / 0.1$  mol% BiCuSeO and  $\text{Cu}_2\text{Se}_{1.020} / 0.3$  mol% BiCuSeO at 973 K are 2.7 and 2.6, increased by 50% and 44.4%, respectively, compared to  $\text{Cu}_2\text{Se}_{1.005}$  ( $ZT_{\text{peak}}=1.8$ ) and  $\text{Cu}_2\text{Se}_{1.020}$  ( $ZT_{\text{peak}}=1.8$ ) (Figure 1(a)). Meanwhile, the average  $ZT$  value ( $ZT_{\text{avg}}$ ) of  $\text{Cu}_2\text{Se}_{1.005} / 0.1$  mol% BiCuSeO and  $\text{Cu}_2\text{Se}_{1.020} / 0.3$  mol% BiCuSeO in the range of 400 K to 973 K is 1.52 and 1.44, increased by 79% and 118%, respectively, compared to  $\text{Cu}_2\text{Se}_{1.005}$  ( $ZT_{\text{avg}}=0.85$ ) and  $\text{Cu}_2\text{Se}_{1.020}$  ( $ZT_{\text{avg}}=0.66$ ).

The repeatability and reproducibility of high  $ZT$  values are often an issue. In this work, the electrical conductivity, Seebeck coefficient, thermal conductivity, and calculated  $ZT$  curves of the composites are shown to be well repeatable and reproducible (Figures S9, S12, S17 and S18). In addition, freshly-prepared samples  $\text{Cu}_2\text{Se}_{1.005} / 0.1$  mol% BiCuSeO and  $\text{Cu}_2\text{Se}_{1.020} /$



---

0.3 mol% BiCuSeO were cross-checked at the University of Michigan (UM, ZEM-3 in Prof. P. F. P. Poudeu's laboratory) and Huazhong University of Science and Technology (HUST, LFA427 in Prof. Junyou Yang's laboratory). The results agree well with ours, within the instrumental errors (**Figure 1(a)**, **Figure S19**).

With the excellent TE performance confirmed, an important question pertains to the stability of Cu<sub>2</sub>Se. To evaluate the stability of the material, measurements of the conductivity of Cu<sup>+</sup> ions and endurance tests under operational conditions of high current density and large temperature difference were performed. A direct-current polarization method with electron-blocking electrodes was utilized to isolate the ionic conduction by filtering electronic conduction. Solid-state Cu|CuBr|Cu<sub>2</sub>Se|CuBr|Cu symmetric pseudo-galvanic cells with the electron blocking CuBr|Cu electrodes were constructed<sup>[41, 42]</sup> (cf. **Figures S20 - S21**). Upon applying a voltage across the composite, keeping the constant current density of ~ 160 mA/cm<sup>2</sup> (i. e., 100 mA DC passing through the sample), the polarization voltage of the pristine Cu<sub>2</sub>Se starts to drop with time, indicating an increased electrical conductivity and thus Cu-precipitation (**Figure 1(b)**). The critical voltage for Cu-precipitation in Cu<sub>2</sub>Se is ~ 0.1 - 0.14 V, consistent with the previous report<sup>[35]</sup>. In sharp contrast, upon incorporating BiCuSeO, the stable polarization voltage increases to above 1.0 V for Cu<sub>2</sub>Se<sub>1.005</sub> / 0.1 mol% BiCuSeO and to 6.0 V for Cu<sub>2</sub>Se<sub>1.020</sub> / 0.3 mol% BiCuSeO (**Figure 1(c) and 1(d)**). This indicates that the

---

incorporation of a small amount of BiCuSeO dramatically improves the stability of the  $\text{Cu}_2\text{Se}$  matrix. In addition, based on the DC polarization measurements, the ionic conductivities of  $\text{Cu}_2\text{Se}$ ,  $\text{Cu}_2\text{Se}_{1.005} / 0.1 \text{ mol\% BiCuSeO}$ , and  $\text{Cu}_2\text{Se}_{1.020} / 0.3 \text{ mol\% BiCuSeO}$  at 693 K were found to be about  $20 \text{ Sm}^{-1}$ ,  $2.2 \text{ Sm}^{-1}$  and  $0.33 \text{ Sm}^{-1}$ , respectively (**Figure 1(b-d)**, **Figure S22**). Evidently, the  $\text{Cu}^+$  conductivity in the composites is suppressed by about two orders of magnitude compared to the pristine  $\text{Cu}_2\text{Se}$ , well accounting for their excellent phase stability and reproducibility.

Another evidence of the improved phase stability comes from the shape of a potential variation curve of the pseudo-galvanic cell. Cu precipitation is the result of an electrochemical reaction that alters the shape of the potential variation curve. In the absence of Cu precipitation, the potential is almost constant over polarization time. However, with Cu metal precipitating (phase segregation), a notable potential drop over time is observed at a fixed current<sup>[41-43]</sup>. Clearly, under a 100 mA, the potential across the pristine  $\text{Cu}_2\text{Se}$  decreases gradually with polarization time, indicating the phase instability with Cu precipitation<sup>[41, 43]</sup>. With the presence of BiCuSeO, however, the potential across  $\text{Cu}_2\text{Se}_{1.005} / 0.1\% \text{ BiCuSeO}$  and  $\text{Cu}_2\text{Se}_{1.020} / 0.3\% \text{ BiCuSeO}$  samples is not only higher but, more importantly, remains constant upon the same high current of 100 mA. This corroborates the excellent phase stability of the composite under a high current flow.

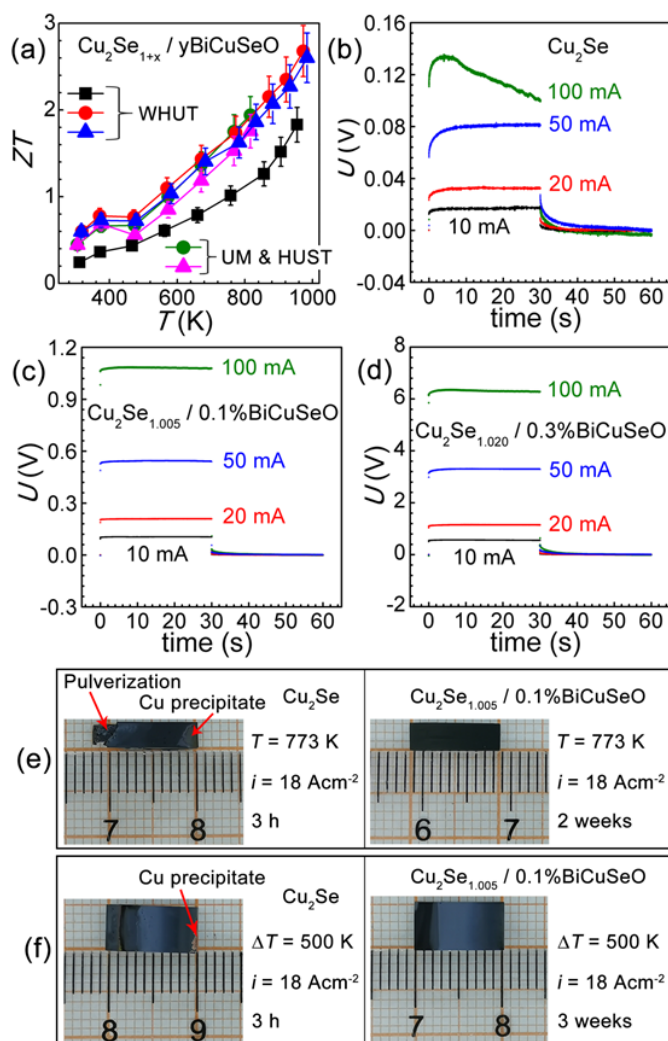
---

Moreover, it is well known that the liquid-like nature of  $\text{Cu}^+$  ions in the  $\beta$ -phase of the  $\text{Cu}_2\text{Se}$  structure destabilizes the material under sufficiently large current densities and/or temperature differences. **Figures 1(e-f)** and **S23 - S33** present the morphology and electrical properties of  $\text{Cu}_2\text{Se}$ ,  $\text{Cu}_2\text{Se}_{1.005}$  / 0.1 mol% BiCuSeO, and  $\text{Cu}_2\text{Se}_{1.020}$  / 0.3 mol% BiCuSeO composites before and after passing a direct current density of  $18 \text{ Acm}^{-2}$  at 773 K, or applying a 500 K temperature gradient (with the high temperature end at 793 K, and the low temperature end at 293 K).

When the current density of  $18 \text{ Acm}^{-2}$  was passed through a pristine  $\text{Cu}_2\text{Se}$  sample at 773 K for 3 h, serious pulverization and Cu precipitation occurred, and the electrical properties of the damaged sample could not be characterized (**Figure S25(a)**). Under the DC current density of  $18 \text{ Acm}^{-2}$  and a temperature difference of 500 K across the sample held for 3 h, massive precipitation of Cu, together with a greatly increased electrical conductivity and decreased Seebeck coefficient (**Figures S30(a), S31**), was observed. This confirms that  $\text{Cu}_2\text{Se}$  is unstable when subjected to large current densities and/or temperature gradients.

The presence of BiCuSeO makes a key difference in the above behavior. For example, the morphology of  $\text{Cu}_2\text{Se}_{1.005}$  / 0.1 mol% BiCuSeO and  $\text{Cu}_2\text{Se}_{1.020}$  / 0.3 mol% BiCuSeO samples showed no discernible change after applying  $18 \text{ Acm}^{-2}$  to the sample for 2 weeks (336 h) at 773 K or imposing a 500 K temperature gradient (**Figure S25(b-c)** and **S30(b-c)**)! Meanwhile,

the electrical conductivity and the Seebeck coefficient measured before and after applying the current and / or the temperature difference returned essentially the same values (Figures S26, S27, S32, and S33). Hence, a trace amount of BiCuSeO as a secondary phase dramatically improves the phase stability of the composite.



This article is protected by copyright. All rights reserved.

---

Figure 1 (a) Temperature dependence of the ZT values of  $\text{Cu}_2\text{Se}_{1+x} / y\text{BiCuSeO}$  composites. Squares, circles and triangles represent  $\text{Cu}_2\text{Se}$ ,  $\text{Cu}_2\text{Se}_{1.005} / 0.1 \text{ mol\% BiCuSeO}$ ,  $\text{Cu}_2\text{Se}_{1.020} / 0.3 \text{ mol\% BiCuSeO}$  samples, respectively. The black, red and blue ones indicate testing at Wuhan University of Technology (WHUT) and the brown and pink ones designate cross checking at the University of Michigan (UM, ZEM-3 in Prof. P. F. P. Poudeu's laboratory) and Huazhong University of Science and Technology (HUST, LFA427 in Prof. Junyou Yang's laboratory). Potential variation curves for  $\text{Cu}_2\text{Se}$  (b),  $\text{Cu}_2\text{Se}_{1.005} / 0.1 \text{ mol\% BiCuSeO}$  (c),  $\text{Cu}_2\text{Se}_{1.020} / 0.3 \text{ mol\% BiCuSeO}$  (d) under different test current at 693 K applied for 30 sec. The resulting ionic conductivities at 693 K of  $\text{Cu}_2\text{Se}$ ,  $\text{Cu}_2\text{Se}_{1.005} / 0.1 \text{ mol\% BiCuSeO}$ ,  $\text{Cu}_2\text{Se}_{1.020} / 0.3 \text{ mol\% BiCuSeO}$  were found to be  $\sim 20 \text{ Sm}^{-1}$ ,  $2.2 \text{ Sm}^{-1}$  and  $0.33 \text{ Sm}^{-1}$ , respectively. (e) Comparison between  $\text{Cu}_2\text{Se}$  and  $\text{Cu}_2\text{Se}_{1.005} / 0.1 \text{ mol\% BiCuSeO}$  when a current of  $18 \text{ Acm}^{-2}$  was passed through at 773 K, (f) Comparison between  $\text{Cu}_2\text{Se}$  and  $\text{Cu}_2\text{Se}_{1.005} / 0.1 \text{ mol\% BiCuSeO}$  while passing a current of  $18 \text{ Acm}^{-2}$  through the samples as well as applying a 500 K temperature gradient ( $T\text{-hot} \sim 793 \text{ K}$ , and  $T\text{-cold} \sim 293 \text{ K}$ ).

How can such a small amount of well dispersed BiCuSeO nanoparticles be so effective in preventing the migration of  $\text{Cu}^+$  ions? In order to reveal the underlying mechanism for this

---

surprising phenomenon, we studied the microstructure and  $\text{Cu}_2\text{Se}/\text{BiCuSeO}$  interface in details from different aspects.

Figures 2(a) - 2(b) show HAADF-STEM images at low magnification and corresponding elemental map (Bi/Cu) of the  $\text{Cu}_2\text{Se}_{1.005} / 0.1\text{mol}\%\text{BiCuSeO}$  bulk material. Apparently, a large number of uniformly distributed pores with sizes ranging from tens of nanometer to several hundred nanometers are observed. The edge of the pores is rich in Bi, indicating BiCuSeO is mainly attached on their inner wall. Such morphology is strongly related to the formation process of BiCuSeO and is common among mesoporous materials prepared by sacrificial template methods<sup>[44]</sup>. In an early work, we have demonstrated the crucial role of  $\text{Bi}_2\text{SeO}_2$  (Figure S34) in the SHS reaction with Cu, and Se to form the nanosized crystals of BiCuSeO (Figure S35 - S36)<sup>[39]</sup> with a polygonal lamellar morphology (Figure S37). It should be mentioned that no Cu metal precipitate was found inside the nano pores of the  $\text{Cu}_2\text{Se}_{1+x} / y\text{BiCuSeO}$  composites before or after the stability measurements under a high current flow or a temperature gradient. Therefore, the uniform distribution of BiCuSeO nanocrystals within the  $\text{Cu}_2\text{Se}$  matrix forms a large number of interfaces which effectively block Cu-ion diffusion. Figure 2(c) shows the HR-STEM image of the interface between  $\text{Cu}_2\text{Se}$  and BiCuSeO in  $\text{Cu}_2\text{Se}_{1.005} / 0.1\text{mol}\%\text{BiCuSeO}$  bulk material around the pore. The electron diffraction for  $\text{Cu}_2\text{Se}$  and BiCuSeO indicates that BiCuSeO epitaxially grows on the (1 3 1) plane of  $\text{Cu}_2\text{Se}$

---

coherently where  $[3 -1 0]$  zone axis of  $\text{Cu}_2\text{Se}$  crystal being parallel with  $[2 2 -1]$  zone axis of  $\text{BiCuSeO}$  crystal. As a result, the  $(0 0 2)$  and  $(1 3 1)$  planes of  $\text{Cu}_2\text{Se}$  are nearly parallel with  $(1 0 2)$  and  $(0 -1 2)$  planes of  $\text{BiCuSeO}$ , respectively. This kind of interface would facilitate the formation of  $\text{Cu}^+$  modulated electric double layer between  $\text{Cu}_2\text{Se}$  and  $\text{BiCuSeO}$ , which plays a key role for stabilizing  $\text{Cu}_2\text{Se}$ .

It is well known that both  $\text{Cu}^+$  ion and hole carriers in  $\text{Cu}_2\text{Se}$  participant in the electric transport. Thus, understanding the role of  $\text{Cu}^+$  ions and the charge transfer at the  $\text{Cu}_2\text{Se}/\text{BiCuSeO}$  interface is the key to revealing the underlying mechanism for the enhanced stability. In order to shed light on the charge transfer at the  $\text{Cu}_2\text{Se}/\text{BiCuSeO}$  heterojunction, the ultraviolet photoemission spectroscopy (UPS) spectra of  $\text{Cu}_2\text{Se}$  and  $\text{BiCuSeO}$  compounds were collected, shown in **Figure 2(d)** and **2(e)**, respectively. The work function of  $\text{Cu}_2\text{Se}$  and  $\text{BiCuSeO}$  are 5.16 eV and 5.52 eV, respectively. The difference in the work function would drive the hole transfer from  $\text{BiCuSeO}$  to  $\text{Cu}_2\text{Se}$ , concomitantly forming a depletion layer with the raw built-in electric field in the  $\text{Cu}_2\text{Se}/\text{BiCuSeO}$  heterojunction pointing from  $\text{Cu}_2\text{Se}$  to  $\text{BiCuSeO}$  (**Figure 2(f)**). This raw built-in electric field in the Schottky heterojunction is also confirmed by a nonlinear feature in  $I-U$  curve (**Figure 2(g)**) in comparison with linearly symmetric  $I-U$  curve of pristine  $\text{Cu}_2\text{Se}$  and pristine  $\text{BiCuSeO}$  (**Figure S39**). This impacts the charge transfer between  $\text{Cu}_2\text{Se}$  and  $\text{BiCuSeO}$ .

---

In order to probe the behavior of charge carrier and  $\text{Cu}^+$  ions at the heterojunction, forward scan and backward scan of  $I-U$  curves were measured with the input voltage in the range from  $-3.5\text{ V}$  to  $3.5\text{ V}$ . Clearly, under the forward scan the current is smaller than that under the reverse scan, regardless of the current directions, resulting in a hysteretic behavior in the  $I-U$  curve (Figure 2(g)). It is well known that the capacitive effect as the Schottky heterojunction can act as a capacitor accumulating charges or  $\text{Cu}^+$  ions at the interface due to the potential difference. However, in the case of the electron capacitor, the current under forward scan should be larger than that under the backward scan, which is opposite to experimental observation in the  $\text{Cu}_2\text{Se}/\text{BiCuSeO}$  heterojunction. Therefore, the hysteretic gap in the  $I-U$  curve of the  $\text{Cu}_2\text{Se}/\text{BiCuSeO}$  heterojunction is predominantly ascribed to capacitive effects of  $\text{Cu}^+$  ions at the interface. The slow reconfiguration process of  $\text{Cu}^+$  ion migration is responsible for the hysteresis in the  $I-U$  curve when the applied voltage is changed. The highly resistive  $\text{BiCuSeO}$  to the passage of  $\text{Cu}^+$  ions, the potential difference between  $\text{Cu}_2\text{Se}$  and  $\text{BiCuSeO}$ , and the unilateral conductivity of the Schottky junction allow accumulation of mobile  $\text{Cu}^+$  ions at the  $\text{Cu}_2\text{Se} / \text{BiCuSeO}$  interfaces under the current flowing from  $\text{Cu}_2\text{Se}$  to  $\text{BiCuSeO}$ . In addition, it is worth noting that due to the unilateral conductivity of the Schottky junction, positive bias voltage allows accumulation of  $\text{Cu}^+$  ions at the interface, while the negative bias voltage expels  $\text{Cu}^+$  ions from the interface and they migrate and redistribute along the current direction in the host matrix. The difference in the  $\text{Cu}^+$  ions concentration in the two sides of



---

the interface region modifies the potential barrier for injection of electronic carrier, leading to the abnormal asymmetry in the  $I-U$  curve of the  $\text{Cu}_2\text{Se}/\text{BiCuSeO}$  heterojunction, which is distinguished from an ideal Schottky junction.

This accumulation of  $\text{Cu}^+$  ions at the interface under the direct current induces interfacial electronic dipole polarization, forming a negatively charged surface on  $\text{BiCuSeO}$  as sketched in **Figure 2(h)**. This is accompanied with the formation of an electric double charge layer and an electrostatic field. The formed space charge region in the  $\text{Cu}_2\text{Se}$  and  $\text{BiCuSeO}$  nano-particle, where  $\text{BiCuSeO}$  nano-particle is equivalent to a positive point charge due to the capacitive effects of  $\text{Cu}^+$  ions, further impedes migration of  $\text{Cu}^+$ . This agrees well with the much lower  $\text{Cu}^+$  conductivity (0.33 S/m vs. 20 S/m for  $\text{Cu}_2\text{Se}$ ) and higher critical voltage ( $> 1$  V vs. 0.13 V for  $\text{Cu}_2\text{Se}$ ) observed in the  $\text{Cu}_2\text{Se}_{1+x} / y\text{BiCuSeO}$  nanocomposites. Furthermore, the increase of external voltage difference between  $\text{Cu}_2\text{Se}$  matrix and  $\text{BiCuSeO}$  nano-particle, drives more  $\text{Cu}^+$  ions to accumulate at the interface, thereby reinforcing the electrostatic field formed in the space charge region. Thus, in spite of the small volume fraction of  $\text{BiCuSeO}$ , the Coulomb force around the  $\text{BiCuSeO}$  nanoparticles effectively blocks long-range motion of  $\text{Cu}^+$  through the sample.

Along with the highly mobile  $\text{Cu}^+$  ions, Cu metal precipitation at the surface and interface is also a major problem for the stability of  $\text{Cu}_2\text{Se}$ . Practically, Cu metal precipitation is an

---

electrochemical reduction reaction process where the highly mobile  $\text{Cu}^+$  ions at the interface or surface close to the upper limit concentration accept electron from the matrix, forming Cu metal<sup>[35]</sup>. Although the aforementioned Schottky  $\text{Cu}_2\text{Se}/\text{BiCuSeO}$  heterojunction facilitates the accumulation of a higher concentration of  $\text{Cu}^+$  ions at the interface over that inside of the matrix, the potential difference in the Schottky junction impedes the electron transfer from  $\text{BiCuSeO}$  to  $\text{Cu}_2\text{Se}$ , unless the energy of electrons is high enough to overcome the potential difference (Figure 2(i)). Therefore, this special heterojunction obstructs the reduction reaction of the  $\text{Cu}^+$  ions accumulated at the interface. Thus, incorporation of  $\text{BiCuSeO}$  not only blocks the long-range migration of  $\text{Cu}^+$  ions throughout the sample but it also imposes a potential barrier for the reduction of  $\text{Cu}^+$  ion into Cu metal. All these effects contribute to the stabilized Cu-ions in the composite.

To gain more insights into the microscopic nature of ionic migration between  $\text{Cu}_2\text{Se}$  and  $\text{BiCuSeO}$ , we conducted an *in situ* transmission electron microscopy study. Figure S40 shows a HAADF image and EDS mapping results for the  $\text{Cu}_2\text{Se}/\text{BiCuSeO}$  heterojunction. As identified by the high resolution image and its corresponding diffraction pattern (Figure S40), the crystal on the left of the heterojunction is  $\text{Cu}_2\text{Se}$ , while the one on the right is  $\text{BiCuSeO}$ . When the current flows from  $\text{BiCuSeO}$  to  $\text{Cu}_2\text{Se}$  (corresponding to the formation of Cu aggregates at the contact point), the critical voltage (threshold) for deposition of Cu metal is

---

1.1 V (**Figure 3(a)**). However, when the current flows in the opposite direction from  $\text{Cu}_2\text{Se}$  to  $\text{BiCuSeO}$  (corresponding to the disappearance of Cu aggregates at the contact point), the critical voltage for rapid  $\text{Cu}^+$  migration is 2.3 V (**Figure 3(b)**). Moreover, no Cu deposition is observed at the  $\text{Cu}_2\text{Se}/\text{BiCuSeO}$  interface despite the fact that the applied reverse voltage is much higher than the forward voltage. Obviously, when the current flows from  $\text{Cu}_2\text{Se}$  to  $\text{BiCuSeO}$ , the electrostatic field formed by the accumulated  $\text{Cu}^+$  ions will oppose migration of  $\text{Cu}^+$  from the  $\text{Cu}_2\text{Se}$  matrix and the Schottky heterojunction of  $\text{Cu}_2\text{Se}/\text{BiCuSeO}$  increases the potential barrier for electron transfer from  $\text{BiCuSeO}$  to  $\text{Cu}_2\text{Se}$ . Hence, the critical voltage for rapid migration of  $\text{Cu}^+$  ions is significantly increased and no Cu deposition is detected. This further corroborates the  $\text{Cu}^+$  ion blocking mechanism in  $\text{Cu}_2\text{Se}_{1+x} / y\text{BiCuSeO}$  composites and the presence of an additional electrostatic field under the current.

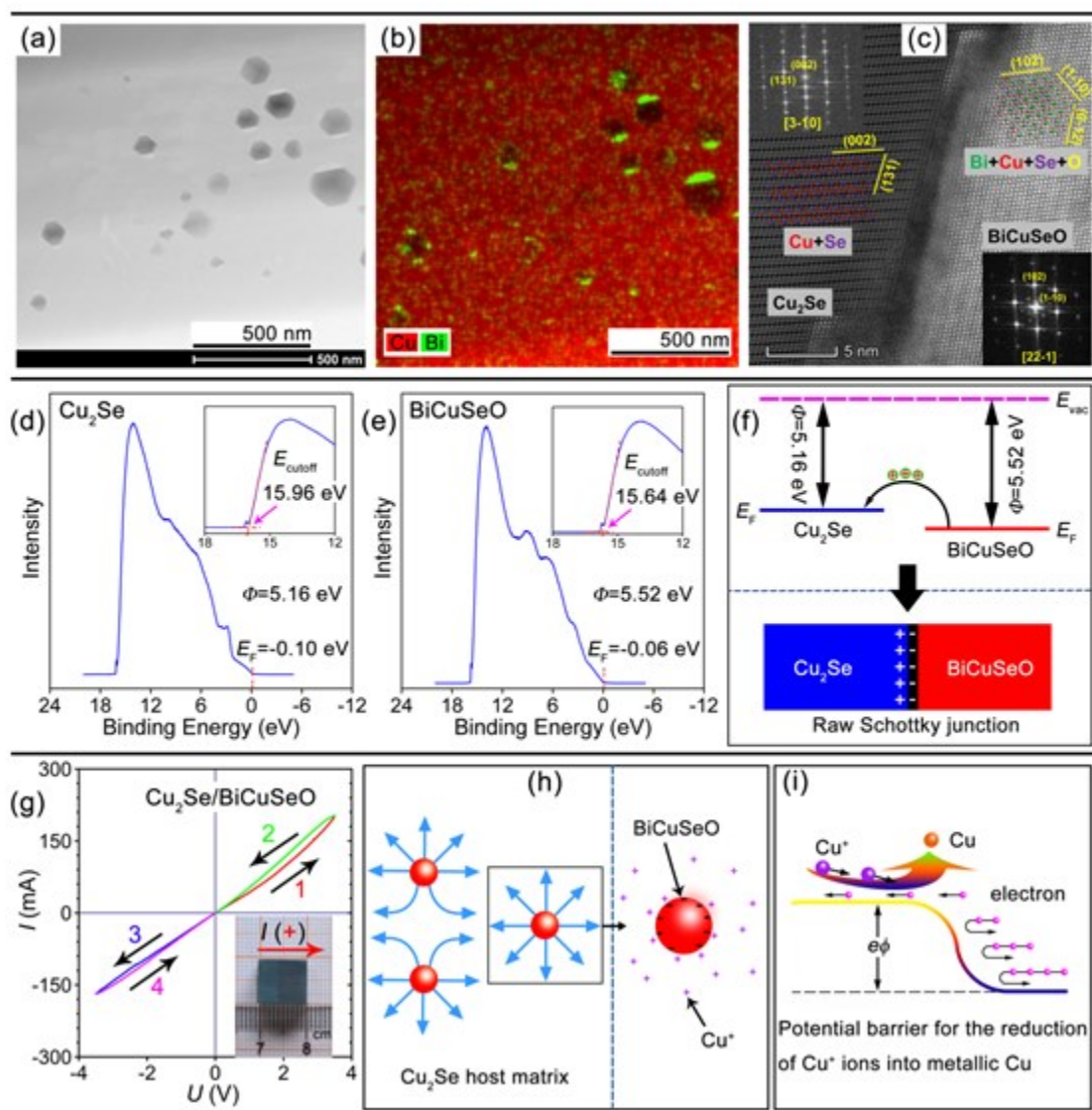


Figure 2. (a) HAADF-STEM image at low magnification of  $\text{Cu}_2\text{Se}_{1.005} / 0.1\text{mol}\%\text{BiCuSeO}$  bulk material, the pores are dark. (b) EDS color elemental map (Bi/Cu) of the whole area in (a). (c) Interface between  $\text{Cu}_2\text{Se}$  and  $\text{BiCuSeO}$  around the pore. Orientation relationship:  $\text{Cu}_2\text{Se} [3 -1 0] // \text{BiCuSeO} [2 2 - 1]$ ,  $\text{Cu}_2\text{Se} (0 0 2) // \text{BiCuSeO} (1 0 2)$ ,  $\text{Cu}_2\text{Se} (1 3 1) // \text{BiCuSeO} (0 -1 2)$ . (d)

---

and (e) Ultraviolet photoemission spectrum (UPS) of the  $\text{Cu}_2\text{Se}$  and  $\text{BiCuSeO}$ . the Fermi edge ( $E_F$ ) is identified in the diagram, and the secondary electron cutoff edge ( $E_{\text{cutoff}}$ ) is highlighted in the illustration. (f) A schematic diagram of hole transfer from  $\text{BiCuSeO}$  to  $\text{Cu}_2\text{Se}$  driven by the difference in their work functions, and the formation of  $\text{Cu}_2\text{Se-BiCuSeO}$  heterojunction, with the direction of the initial built-in electric field pointing from  $\text{Cu}_2\text{Se}$  to  $\text{BiCuSeO}$ . (g)  $I-U$  curve of a  $\text{Cu}_2\text{Se/BiCuSeO}$  heterojunction. Clearly, a nonlinear  $I-U$  curve and hysteresis are observed. (h) Schematic illustration of the long range electrostatic field formation and the space charge distribution in electric double layer around  $\text{BiCuSeO}$  in the  $\text{Cu}_2\text{Se}_{1+x} / y\text{BiCuSeO}$  composites. A small amount of  $\text{Cu}^+$  ions accumulate at the interface between  $\text{Cu}_2\text{Se}_{1+x}$  matrix and  $\text{BiCuSeO}$  under an external current. This induces interfacial electronic dipole polarization, leading to negatively charged  $\text{BiCuSeO}$  surfaces. The formed space charge region in the  $\text{Cu}_2\text{Se}$  and  $\text{BiCuSeO}$  nanoparticle, where the  $\text{BiCuSeO}$  nanoparticle is equivalent to a positive point charge due to the capacitive effects of  $\text{Cu}^+$  ions. Thus, in spite of a small volume fraction of  $\text{BiCuSeO}$ , the long-range Coulomb force around  $\text{BiCuSeO}$  nanoparticles effectively blocks motion of  $\text{Cu}^+$  through the sample. (i) A schematic diagram of potential barrier in the Schottky heterojunction, which obstructs the reduction reaction from  $\text{Cu}^+$  into  $\text{Cu}$  metal.

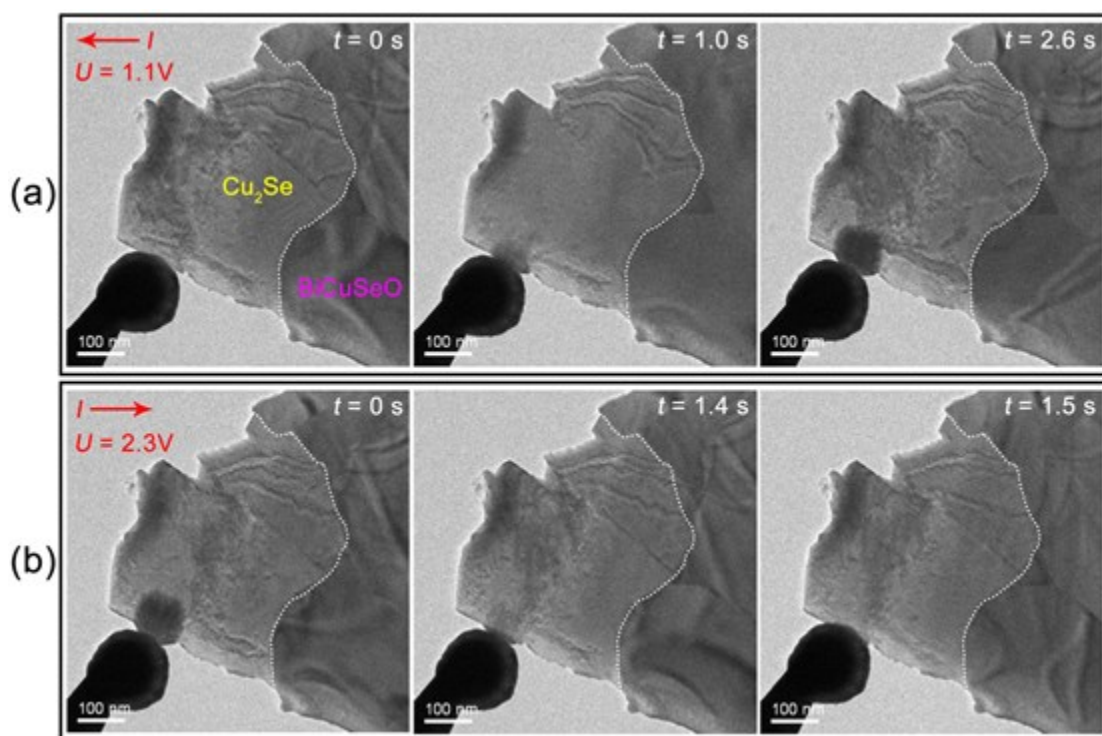


Figure 3 In situ transmission electron microscopy images, (a) Different stages (in time) during the current flow from BiCuSeO to Cu<sub>2</sub>Se. The developing black spot in the vicinity of the contact is the precipitated copper, which is observed when the applied voltage reaches the critical value of 1.1 V. (b) Different stages following the current reversal (the current now flows from Cu<sub>2</sub>Se to BiCuSeO). In this case, the critical voltage for rapid migration of Cu<sup>+</sup> (i.e., the disappearance of the previously precipitated copper) is 2.3 V.

Obviously, the Cu<sup>+</sup> modulated electric double layer in the space charge region between the Cu<sub>2</sub>Se and BiCuSeO phases blocks the long-range ion migration in the entire sample. Along

---

with the Schottky junction, which prevents electron transfer from BiCuSeO to Cu<sub>2</sub>Se and thus hinders the reduction reaction, the high TE performance of the Cu<sub>2</sub>Se/BiCuSeO composites is stabilized. Additionally, the TE performance of Cu<sub>2</sub>Se / BiCuSeO composites is strongly related to its carrier concentration that is determined by the Cu content, i.e., Cu vacancies in the Cu<sub>2</sub>Se host. We now discuss the mechanism for modulation of the carrier concentration.

The regulating behavior of the Cu/Se content in the host matrix is confirmed by DSC tests performed on the as-prepared composites (**Figure 4(a)** and **Figure S41**). For Cu<sub>2</sub>Se<sub>1+x</sub>, the phase transition temperature ( $T_{tr}$ ) decreases from 399.2 K to 387.4 K as the content of Se increases. For Cu<sub>2</sub>Se / yBiCuSeO, Cu<sub>2</sub>Se<sub>1.005</sub> / yBiCuSeO, and Cu<sub>2</sub>Se<sub>1.010</sub> / yBiCuSeO, the  $T_{tr}$  tends to shift to a lower temperature, indicating the decreased Cu/Se ratio in the matrix according to the binary Cu-Se phase diagram<sup>[45]</sup>. For Cu<sub>2</sub>Se<sub>1.015</sub> / yBiCuSeO and Cu<sub>2</sub>Se<sub>1.020</sub> / yBiCuSeO,  $T_{tr}$  tends to shift to a higher temperature, implying an increased Cu/Se ratio in the matrix. The DSC results indicate that the presence of Cu<sup>+</sup> vacancies inter-diffusion process during the preparation of Cu<sub>2</sub>Se/BiCuSeO composite can modulate the copper content in the host matrix. This helps to maintain the carrier concentration at the optimal region over a wide range of compositions, which is very important for the reproducible synthesis of materials on a large scale.

---

To reveal and substantiate the mechanism underlying the high TE performance of these composites, low temperature and high temperature transport properties were studied (Figures S4, S6, S8, S11, S14, S16, S42 and S43). Specifically, Figure 4(b) shows the relation between the carrier concentration and the composition (x, y) at 600 K. As shown, the optimal carrier concentrations are in the range of  $1.0 - 1.5 \times 10^{21} \text{ cm}^{-3}$ , which yields peak  $ZT$  values exceeding 2.0. To more clearly see the self-regulation of the carrier concentration by BiCuSeO and Se excess, we present a baseline (red dotted line) derived by assuming that each excess Se atom donates two holes to the composite. Apparently, the presence of BiCuSeO tends to increase (decrease) the carrier concentration when  $x \leq 0.01$  (when  $x > 0.01$ ). Since the carrier concentration is positively related to the x-value, the presence of BiCuSeO thus self-regulates the carrier concentration. The pivotal (balance) point is near  $x = 0.01$ , where the carrier concentration is around  $1.0 \times 10^{21} \text{ cm}^{-3}$ , close to the lower end of the optimal carrier concentration. It remains an open question how this optimized carrier concentration is achieved over such a wide range of compositions and how it is coordinated with the effectively regulating behavior of Cu vacancies between  $\text{Cu}_2\text{Se}$  and BiCuSeO during the preparation process.



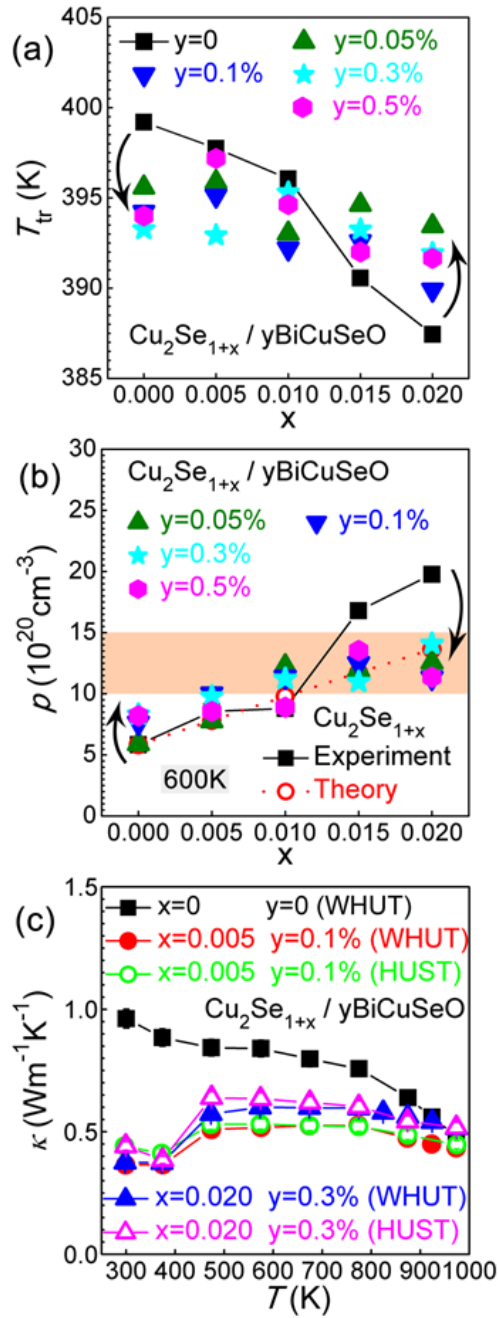


Figure 4 (a) Relationship between the phase transition temperature and composition of composite structures. (b) Relationship between the carrier concentration ( $\rho$ ) of holes and

---

*composition of composite structures. The orange region corresponds to the optimal carrier concentration, which yields ZT values exceeding 2.0. Clearly, the incorporation of BiCuSeO can adjust the relative content of copper in the Cu<sub>2</sub>Se matrix (as seen in the variation of the phase transition temperature), which, in turn, adjusts the carrier concentration to optimal in a wide range of compositions. (c) Temperature dependence of the total thermal conductivity (k) of Cu<sub>2</sub>Se<sub>1+x</sub> / yBiCuSeO composites. Squares, circles and triangles represent Cu<sub>2</sub>Se, Cu<sub>2</sub>Se<sub>1.005</sub> / 0.1 mol% BiCuSeO, Cu<sub>2</sub>Se<sub>1.020</sub> / 0.3 mol% BiCuSeO samples, respectively. The solid symbols indicate testing at the Wuhan University of Technology (WHUT) while the open symbols designate cross checking at Huazhong University of Science and Technology (HUST, LFA427 in Prof. Junyou Yang's laboratory)*

The origin of charge carriers (holes) in Cu<sub>2</sub>Se and BiCuSeO is Cu vacancies<sup>[4, 46]</sup>. Actually, the carrier concentration of Cu<sub>2</sub>Se is about  $4 \times 10^{20} \text{ cm}^{-3}$  due to the Cu vacancies and that of BiCuSeO is about  $2 \times 10^{17} \text{ cm}^{-3}$  at room temperature<sup>[4, 7, 39]</sup>. Therefore, driven by the Cu vacancy potential difference, Cu vacancies naturally diffuses from BiCuSeO to Cu<sub>2</sub>Se in the Cu<sub>2</sub>Se<sub>1+x</sub> / yBiCuSeO composite when  $x \leq 0.01$ , and then diffuses from Cu<sub>2</sub>Se to BiCuSeO when  $x \geq 0.01$ . This points to the effective regulation of the relative copper content in the host matrix.

---

The remarkable reduction of the already low thermal conductivity of  $\text{Cu}_2\text{Se}$  in the composite samples is a contributing factor to the high TE performance. As noticed, the  $\text{Cu}_2\text{Se}_{1+x}$  /  $\text{yBiCuSeO}$  nanocomposites exhibits low thermal conductivity (**Figure 4(c)**), especially at some particular compositions, *e.g.*  $\text{Cu}_2\text{Se}_{1.005}$  / 0.1 mol%  $\text{BiCuSeO}$  (**Figure S7**),  $\text{Cu}_2\text{Se}_{1.010}$  / 0.3 mol%  $\text{BiCuSeO}$  (**Figure S10**),  $\text{Cu}_2\text{Se}_{1.015}$  / 0.1 mol%  $\text{BiCuSeO}$  (**Figure S13**),  $\text{Cu}_2\text{Se}_{1.020}$  / 0.1 mol%  $\text{BiCuSeO}$ , and  $\text{Cu}_2\text{Se}_{1.02}$  / 0.3 mol%  $\text{BiCuSeO}$  (**Figure S15**). It should be noted that the low thermal conductivity was crosschecked by other group (HUST).

The exact origin of the ultra-low thermal conductivity in  $\text{Cu}_2\text{Se}$ , however, has been the subject of debate. Several different theories have been proposed. For example, some investigations show that the liquid-like diffusion of  $\text{Cu}^+$  ions suppresses the transverse phonons, leading to a dramatically reduced thermal conductivity. They conclude that the higher the ionic conductivity, the lower the thermal conductivity. In contrast, other investigations show that migration of  $\text{Cu}^+$  ions cannot prevent the propagation of transverse acoustical phonons, and argue that the lattice anharmonicity, correlated with the diffusion of  $\text{Cu}^+$  (diffusion rate and hopping time), is the main origin of the low thermal conductivity<sup>[47]</sup>. In the context of our experimental data, the decrease in the ionic migration in the samples upon incorporating  $\text{BiCuSeO}$  nano-particles is unequivocal. This modified process of dynamic  $\text{Cu}^+$  ions may intensify phonon scattering, suppressing the lattice thermal conductivity<sup>[47, 48]</sup>. Moreover,

---

BiCuSeO nanoparticles and nano pores enhance interfacial phonon scattering and strongly scatter the heat-carrying phonons, resulting in an additional reduction of the thermal conductivity and thus high  $ZT$  in  $\text{Cu}_2\text{Se}_{1+x} / y\text{BiCuSeO}$  composites.

### 3. CONCLUDING REMARKS

Through an *in situ* incorporation of nanoparticles of BiCuSeO, the superionic nature of  $\text{Cu}_2\text{Se}$  in macroscopic samples was largely eliminated while maintaining excellent TE properties.

The superior phase and physical property stability is realized by creating an ion-modulated interfacial electrostatic field under the direct current that blocks the long-range migration of  $\text{Cu}^+$  ions across  $\text{Cu}_2\text{Se}_{1+x} / \text{BiCuSeO}$  interfaces and prevents the reduction reaction from  $\text{Cu}^+$

to Cu metal. Meanwhile, the effective regulation of the relative content of copper and the concentration of holes in the host matrix through inter-diffusion of Cu vacancies between the

$\text{Cu}_2\text{Se}_{1+x}$  host matrix and the BiCuSeO nanophase during the synthesis process maintains

high power factor and the carrier concentration at the optimal carrier concentration range over a wide temperature and composition region. These effects stabilize the excellent TE

performance under high current/voltage and/or large temperature gradient. Moreover, the

lattice phonons are strongly scattered by BiCuSeO nanoparticles and nano pores,

dramatically reducing the lattice thermal conductivity. Owing to the optimal hole concentration

---

and the dramatically suppressed thermal conductivity, the  $\text{Cu}_2\text{Se}_{1+x} / y\text{BiCuSeO}$  composites attain high peak  $ZT$ s of  $\sim 2.7$  at 973 K, and the corresponding average  $ZT$  values between 400 K and 973 K reach a high value of 1.5. The excellent repeatability and reproducibility of TE properties strongly substantiate the proposed mechanism. The results highlight a new strategy for the active control of ion migration and may have broader implications for the stabilization of other systems such as halide perovskites and solid state interfacial behavior in solid state batteries and fuel cells.

## ASSOCIATED CONTENT

### Supporting information

Synthesis of  $\text{Cu}_2\text{Se}_{1+x} / y\text{BiCuSeO}$  composites

Figures S1 - S43

3D reconstruction for a pit of  $\text{Cu}_2\text{Se}_{1.005} / 0.1\% \text{BiCuSeO}$  composite

*In situ* transmission electron microscopy.

The supporting information is available free of charge from the internet or from the authors.

## AUTHOR INFORMATION

This article is protected by copyright. All rights reserved.

---

## Corresponding Author

\*E-mail: jihui@uw.edu, m-kanatzidis@northwestern.edu, tangxf@whut.edu.cn.

## Author Contributions

All authors have given approval to the final version of the manuscript.

## Notes

The authors declare no competing financial interest.

## ACKNOWLEDGEMENTS

We acknowledge support from the National Key Research and Development Program of China (2019YFA0704900), the Natural Science Foundation of China (Grant No. 51972256, 51632006, 51521001 and 51872219), and the 111 Project of China (Grant No. B07040).

Dongwang Yang is grateful to Prof. Wenyu Zhao and Mr. Shifang Ma for their help with high temperature Hall coefficient measurement at State Key Laboratory of Advanced Technology for Materials Synthesis and Processing in Wuhan University of Technology, to Prof. P. F. P. Poudeu and Mr. Ruiming Lu for crosschecking with high temperature electrical properties measurement in the University of Michigan, to Prof. Junyou Yang and Mr. Jiwu Xin for crosschecking with high temperature thermal properties measurement in Huazhong University of Science and Technology, to Prof. Jianbo Wang and Mr. Yuanlin Zhuang for their

This article is protected by copyright. All rights reserved.

---

help with thinning of in-situ electron microscopy samples by focused ion beam (FIB) in Wuhan University, to Dr. De Fang for help with UPS measurement in Materials Research and Test Center of Wuhan University of Technology. The S/TEM work was performed at the Nanostructure Research Center (NRC), which is supported by the Fundamental Research Funds for the Central Universities (WUT: 2019III012GX, 2020III002GX), the State Key Laboratory of Advanced Technology for Materials Synthesis and Processing, and the State Key Laboratory of Silicate Materials for Architectures (all of the laboratories are at Wuhan University of Technology). Work at Northwestern University was supported by the Department of Energy, Office of Science Basic Energy Sciences under grant DE-SC0014520, DOE Office of Science (sample preparation, synthesis, XRD, TE measurements). J. Y acknowledges the support by the Inamori Foundation.

## REFERENCES

1. D. M. Rowe, *CRC Handbook of Thermoelectrics*, CRC Press, Boca Raton, 1995.
2. H. J. Goldsmid, *Introduction to Thermoelectricity*, Springer, 2010.
3. J. He and T. M. Tritt, *Science*, 2017, 357, 1369.

This article is protected by copyright. All rights reserved.

- 
4. H. L. Liu, X. Shi, F. F. Xu, L. L. Zhang, W. Q. Zhang, L. D. Chen, Q. Li, C. Uher, T. Day and G. J. Snyder, *Nat Mater*, 2012, 11, 422.
5. R. Nunna, P. F. Qiu, M. J. Yin, H. Y. Chen and L. D. Chen, *Energy Environ. Sci.*, 2017, 10, 1928.
6. A. A. Olvera, N. A. Moroz, P. Sahoo, P. Ren, T. P. Bailey, A. A. Page, C. Uher and P. F. P. Poudeu, *Energy Environ. Sci.*, 2017, 10, 1668.
7. X. L. Su, F. Fu, Y. G. Yan, G. Zheng, T. Liang, Q. Zhang, X. Cheng, D. W. Yang, H. Chi, X. F. Tang, Q. J. Zhang and C. Uher, *Nat Commun*, 2014, 5, 4908.
8. Y. He, T. Day, T. S. Zhang, H. L. Liu, X. Shi, L. D. Chen and G. J. Snyder, *Adv. Mater.*, 2014, 26, 3974.
9. Y. He, P. Lu, X. Shi, F. F. Xu, T. S. Zhang, G. J. Snyder, C. Uher and L. D. Chen, *Adv. Mater.*, 2015, 27, 3639.
10. X. X. Xiao, W. J. Xie, X. F. Tang and Q. J. Zhang, *Chinese Phys. B*, 2011, 20, 340.
11. G. J. Snyder, M. Christensen, E. Nishibori, T. Caillat and B. B. Iversen, *Nat. Mater.*, 2004, 3, 458.



- 
12. T. Caillat, J. P. Fleurial and A. Borshchevsky, *J. Phys. Chem. Solids*, 1997, **58**, 1119.
13. M. Ferhat and J. Nagao, *J. Appl. Phys.*, 2000, **88**, 813.
14. Y. F. Ding, Y. Qiu, K. F. Cai, Q. Yao, S. Chen, L. D. Chen and J. Q. He, *Nat. Commun.*, 2019, **10**, 841.
15. Y. Z. Pei, N. A. Heinz and G. J. Snyder, *J. Mater. Chem.*, 2011, **21**, 18256.
16. D. W. Yang, X. L. Su, F. C. Meng, S. Wang, Y. G. Yan, J. H. Yang, J. He, Q. J. Zhang, C. Uher, M. G. Kanatzidis and X. F. Tang, *J. Mater. Chem. A*, 2017, **5**, 23243.
17. X. Shi, H. Y. Chen, F. Hao, R. H. Liu, T. Wang, P. F. Qiu, U. Burkhardt, Y. Grin and L. Chen, *Nat. Mater.*, 2018, **17**, 421.
18. B. Li, H. Wang, Y. Kawakita, Q. Zhang, M. Feygenson, H. L. Yu, D. Wu, K. Ohara, T. Kikuchi, K. Shibata, T. Yamada, X. K. Ning, Y. Chen, J. Q. He, D. Vaknin, R. Q. Wu, K. J. Nakajima and M. G. Kanatzidis, *Nat. Mater.*, 2018, **17**, 226.
19. J. L. Niedziela, D. Bansal, A. F. May, J. X. Ding, T. Lanigan-Atkins, G. Ehlers, D. L. Abernathy, A. Said and O. Delaire, *Nat. Phys.*, 2019, **15**, 73.

- 
20. W. Li, S. Q. Lin, B. H. Ge, J. Yang, W. Q. Zhang and Y. Z. Pei, *Adv. Sci.*, 2016, **3**, 1600196.
21. W. F. Kuhs, R. Nitsche and K. Scheunemann, *Mater. Res. Bull.*, 1979, **14**, 241.
22. X. Shen, C. C. Yang, Y. M. Liu, G. W. Wang, H. Tan, Y. H. Tung, G. Y. Wang, X. Lu, J. He and X. Y. Zhou, *ACS Appl. Mater. Inter.*, 2018, **11**, 2168.
23. W. Li, S. Q. Lin, M. Weiss, Z. W. Chen, J. Li, Y. D. Xu, W. G. Zeier and Y. Z. Pei, *Adv. Energy Mater.*, 2018, **8**, 1800030.
24. S. Q. Lin, W. Li, S. Li, X. Zhang, Z. Chen, Y. Xu, Y. Chen and Y. Pei, *Joule*, 2017, **1**, 816.
25. B. Jiang, P. Qiu, H. Chen, Q. Zhang, K. Zhao, D. Ren, X. Shi and L. Chen, *Chemical Communications*, 2017, **53**, 11658.
26. T. P. Bailey and C. Uher, *Current Opinion in Green and Sustainable Chemistry*, 2017, **4**, 58.
27. E. F. Hampl Jr, Minnesota Mining and Mfg. Co., St. Paul (USA). Technical Ceramic Products Div., 1976.
28. N. B. Elsner and J. Chin, General Atomic Co., San Diego, Calif. (USA), 1975.

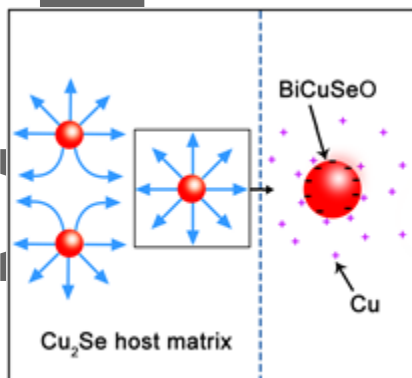
- 
29. C. J. Goebel and T. E. Hammel, Teledyne Co., Program final report (NO. TES-33009-46), 1978.
30. G. Stapfer and V. C. Truscello, Report NO. 19770066000, NASA JPL, 1977.
31. G. Stapfer, Jet Propulsion Lab., Pasadena, CA (USA), 1977.
32. T. P. Bailey, H. Si, H. Y. Xie, A. Olvera, P. F. P. Poudeu, X. F. Tang and C. Uher, *J. Mater. Chem. A*, 2016, **4**, 17225.
33. G. Dennler, R. Chmielowski, S. Jacob, F. Capet, P. Roussel, S. Zastrow, K. Nielsch, I. Opahle and G. K. H. Madsen, *Adv. Energy Mater.*, 2014, **4**, 1301581.
34. D. R. Brown, T. Day, T. Caillat and G. J. Snyder, *J. Electron. Mater.*, 2013, **42**, 2014.
35. P. F. Qiu, M. T. Agne, Y. Y. Liu, Y. Q. Zhu, H. Y. Chen, T. Mao, J. Yang, W. Q. Zhang, S. M. Haile, W. G. Zeier, J. Janek, C. Uher, X. Shi, L. D. Chen, G. J. Snyder, *Nat. Commun.*, 2018, **9**, 2910.
36. P. F. Qiu, T. Mao, Z. F. Huang, X. G. Xia, J. C. Liao, M. T. Agne, M. Gu, Q. H. Zhang, D. D. Ren, S. Q. Bai, X. Shi, G. J. Snyder and L. D. Chen, *Joule*, 2019, **3**, 1.
37. A. G. Merzhanov, *Arch. Combustionis*, 1981, **1**, 23.

- 
38. A. G. Merzhanov, *Combust. Sci. Technol.*, 1994, **98**, 307.
39. D. W. Yang, X. L. Su, Y. G. Yan, T. Z. Hu, H. Y. Xie, J. He, C. Uher, M. G. Kanatzidis and X. F. Tang, *Chem. Mater.*, 2016, **28**, 4628.
40. W. J. Qiu, P. Lu, X. Yuan, F. F. Xu, L. H. Wu, X. Z. Ke, H. L. Liu, J. Yang, X. Shi, L. D. Chen, J. H. Yang, W. Q. Zhnag, *J. Chem. Phys.*, 2016, **144**, 194502.
41. I. Yokota, *J Phys. Soc. Jpn.*, 1953, **8**, 595.
42. I. Yokota, *J. Phys. Soc. Jpn.*, 1961, **16**, 2213.
43. Y. Y. Liu, P. F. Qiu, H. Y. Chen, R. Chen, X. Shi and L. D. Chen, *J. Inorg. Mater.*, 2017, **32**, 1337.
44. M. Oschatz, J. T. Lee, H. Kim, W. Nickel, L. Borchardt, W. I. Cho, C. Ziegler, S. Kaskel and G. Yushin, *J. Mater. Chem.*, 2014, **A 2**, 17649.
45. V. M. Glazov, A. S. Pashinkin and V. A. Fedorov, *Inorg. Mater.*, 2000, **36**, 641.
46. L. D. Zhao, J. Q. He, D. Berardan, Y. H. Lin, J. F. Li, C. W. Nan and N. Dragoe, *Energy Environ. Sci.*, 2014, **7**, 2900.
47. D. J. Voneshen, H. C. Walker, K. Refson and J. P. Goff, *Phys. Rev. Lett.*, 2017, **118**, 145901.

---

48. X. Liang, *Appl. Phys. Lett.*, 2017, 111, 133902.

The space charge region between the  $\text{Cu}_2\text{Se}$  host matrix and *in situ* formed  $\text{BiCuSeO}$  under a direct current causes drastic suppression of  $\text{Cu}^+$  ion migration in the composites, and obstructs the reduction reaction of  $\text{Cu}^+$  into Cu metal, which, together with the effective regulation of carrier concentration as well as enhanced interfacial phonon scattering, greatly stabilizes the improved thermoelectric performance.



This article is protected by copyright. All rights reserved.